Measuring Transit Timing Variations of Exoplanets using Small Telescopes

Caroline V. Morley*

MIT Department of Earth Atmosphere and Planetary Science; MIT Department of Physics

(Dated: May 7, 2010)

Transits of exoplanets were observed from June 2009 through January 2010. Six transit light curves are presented in this paper for three planets: WASP-10b, WASP-11/HAT-P-10b, and TrES-3. Measurements of the planetary radii, semi-major axis, transit duration, and period confirmed literature values to within two sigma. Transit timing variations were not observed in these systems, but calculations show that it would be possible to measure transit timing variations induced by large exomoons (greater than about 6 Earth masses) in the WASP-11/HAT-P-10b system. Challenges of exoplanet observation from small telescopes are discussed. It was determined that overall, transit measurements of many exoplanets using small telescopes can be successful and scientifically useful.

*cmorley@mit.edu

ACKNOWLEDGMENTS

I would like to thank my thesis advisor, Jim Elliot, for all of his help and wisdom during this project.

I would like to extend a huge thank you to Elisabeth Adams, for everything she taught me during this process. She guided me through the project, from my first astronomical observations ever, to data reduction and analysis, to last-minute thesis revisions from her vacation in Europe. Without all of Elisabeth's time, effort, and Mathematica code, this project would never have happened.

I would like to thank Tim Brothers for taking care of all the Wallace telescopes and being very patient when things occasionally went wrong.

I would like to thank Jane Connor for all of her writing help and support.

I would also like to thank Scott Morrison for observing with me, driving me home from observation runs, helping me with LaTeX (and grammar), and for generally being patient and good-humored even when I was not.

CONTENTS

I. INTRODUCTION

I.1. Scientific Background: Transiting Exoplanets

The study of extrasolar planets is a new and dynamic field of research. The first planets around other stars were discovered in the early 1990s, and as of May 2010, scientists have discovered 453 exoplanets[1]. Different methods of detection allow researchers to determine different planetary parameters. For instance, radial velocity measurements are made using the doppler shifts in the star's spectrum from its motion about the center of mass of the system; these measurements allow scientists to calculate minimum mass of a planet (the mass multiplied by the sine of the orbital inclination).

Of the known exoplanets, 79 are known to transit — or cross in front of — the central star[1]. Using the light curve of a transit, the ratio of the radius of the planet to the radius of its host star can also be determined. A transiting planet blocks a percentage of light from the star during the transit; the change in flux from the star during transits observed to date varies between 2.8% and 0.3%[1]. A schematic depicting a transiting planet and its light curve is shown in Figure 1, where the curve shows a small decrease in flux.

By combining the mass, determined using radial velocity calculations, and the radius, determined from the transit light curve, the density of the planet can be calculated. From the density, constraints on the planet's composition can be determined.

Other parameters of the system can also be calculated from the observation of a transit. Orbital parameters such as period and semi-major axis can be determined by measuring the shape of a light curve. Also, the shape of the light curve is different in different wavelengths, a phenomenon caused by a stellar property called limb darkening. Limb darkening refers

[1] *The Extrasolar Planets Encyclopaedia.* Web. 02 May 2010. http://exoplanet.eu/

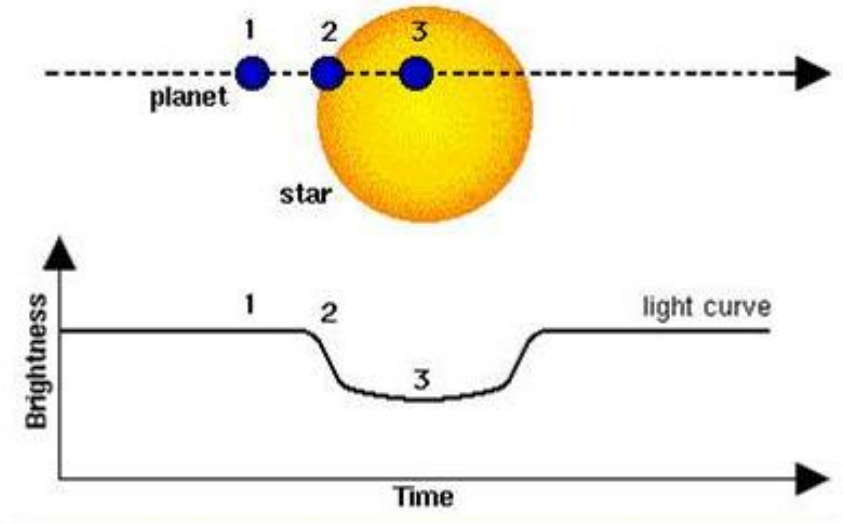

FIG. 1. **Schematic of Transiting Planet.** This image shows an artist's depiction of a transit. The light curve on the bottom shows how the flux from the star decreases by a small percentage for the duration of time that the planet blocks the light of a small section of the star. The numbers on the image and light curve correspond to moments in time before and during the transit (Centre National D'etudes Spatiales)

to the fact that because the temperature of the star decreases as a function of increasing radius within a star, the center of the star's disk appears to radiate at bluer wavelengths than the edge of a star. In general, limb darkening effects cause transits measured in red wavelengths to have light curves with a flatter bottom section than transits measured in blue wavelengths, because the star is more uniformly bright at redder wavelengths.

Another quantity that can be measured is the midtime of the transit. By comparing this value to the midtimes of previously measured transits, any variability in the period can be constrained. These variations, called Transit Timing Variations or TTV, would indicate the presence of a perturbing body in the system (Holman & Murray, 2005). For instance, another planet in the system or a large moon around the planet could be detected. Upper constraints on the mass of such a perturbing object can be made.

The limits of extrasolar planet observation from Wallace Observatory were determined.

This determination was challenging because the variability of the weather was a dominating factor in observations, but some conclusions were drawn about the viability of exoplanet research at Wallace. In particular, the precision of timing of transits that can be determined from Wallace data was determined. This is a particularly interesting question because the telescopes at Wallace Observatory are similar to telescopes generally used by amateur observers. There are many thousands of amateur telescopes across the country, and I quantified the precision of transit timing variations (TTV) that they can achieve using this equipment. Using this value and calculations to determine where viable moons could exist in the system, I calculated a lower bound for the mass of a detectable "exomoon" (moon around an exoplanet) around specific planets in my study. If detections of TTV could be made using small telescopes, amateurs could play an extremely important role in discovering planets or moons in known transiting systems.

I.2. Earlier Research on Observed Exoplanets

I.2.1. WASP-10b

WASP-10 (GSC 2752-00114) is a relatively faint star (V = 12.7) located about 90 parsecs from the Earth (Christian et al. 2009). Stellar parameters for WASP-10 are summarized in Table I.

TABLE I. Stellar Parameters for WASP-10 from Christian et al. 2009

Parameter	Value
RA (J2000) (h min s)	23 15 58.3
Dec. (J2000) (° min s)	+31 27 46.4
V (Magnitude)	12.7
Distance (parsec)	90 ±20
T_{eff} (K)	4675 ± 100

WASP-10b is a 'hot Jupiter' discovered by the Wide Angle Search for Planets (WASP) Consortium (Christian et al., 2009). This type of planet is called a 'hot Jupiter' because it is similar in mass to Jupiter, but it orbits much closer to the star, making the planet much hotter than Jupiter. Johnson et al. (2009) suggested that the system had slightly different planetary parameters than those given by Christian et al. (2009). Johnson et al. included precision photometry taken using the novel Orthogonal Parallel Transfer Imaging Camera, mounted on the University of Hawaii 2.2 m telescope atop Mauna Kea, Hawaii. The revised value for the radius of the planet was 16% smaller than in the previous paper. A summary of important parameters is shown in Table II.

TABLE II. Literature Values for WASP-10b from Discovery and Follow-up Papers

Parameter	Christian et al. 2009	Johnson et al. 2009
Transit Epoch (BJD)	$2454357.85808\ ^{+0.00041}_{-0.00036}$	$2454664.030913 \pm 0.000082$
Orbital Period (days)	$3.0927636\ ^{+0.0000094}_{-0.000021}$	3.0927616 ± 0.0000112
Planet/star area ratio	$0.029\ ^{+0.001}_{-0.001}$	$0.02525\ ^{+0.00024}_{-0.00028}$
Planet radius (R_J)	$1.28\ ^{+0.077}_{-0.091}$	1.080 ± 0.020
Transit duration (hours)	$2.356344\ ^{+0.0456}_{-0.036}$	$2.2271^{+0.0078}_{-0.0068}$
Impact parameter	$0.568\ ^{+0.054}_{-0.084}$	$0.299\ ^{+0.029}_{-0.043}$
Planet mass (M_J)	$2.96\ ^{+0.22}_{-0.17}$	$3.15^{+0.13}_{-0.11}$
Orbital semimajor axis (AU)	$0.0369\ ^{+0.0012}_{-0.0014}$	$0.03781\ ^{+0.00067}_{-0.00047}$

I.2.2. TrES-3

TrES-3 (GSC 03089-00929) is a 12.4 magnitude G type star. It is located about 400 parsecs from the Solar System (O'Donovan et al., 2007). Stellar parameters for TrES-3 are summarized in Table III.

TABLE III. Stellar Parameters for TrES-3 from O'Donovan et al., 2007

Parameter	Value
RA (J2000) (h min s)	17 52 07.03
Dec. (J2000) (° min s)	+37 32 46.1
V (Magnitude)	12.402 ± 0.006
Distance (parsec)	400 ± 200
$T_{\rm eff}$ (K)	5720 ± 150

The name TrES-3 also applies to the exoplanet discovered around this star. It was discovered by the Trans-atlantic Exoplanet Survey (TrES) network; O'Donovan et at. announced the discovery in 2007. TrES-3 is a massive 'hot Jupiter' with a very short orbital period (1.30619 days). TrES-3 is located 0.0226 ± 0.0013 AU from the central star (for reference, the distance from the Sun to Mercury is about 0.39 AU). A summary of the literature values of important transit parameters is shown in Table IV.

TABLE IV. Literature Values from TrES-3 Discovery and Follow-up Papers

Parameter	O'Donovan 2007	Sozzetti 2008
Transit Epoch (BJD)	2454185.9101 ± 0.0003	2454594.745943 ± 0.000253
Orbital Period (days)	1.30619 ± 0.00001	1.30618581
Planet/star radius ratio	0.1660 ± 0.0024	0.1655±0.0020
Planet radius (R_J)	1.295 ± 0.081	$1.336^{+0.031}_{-0.037}$
Impact parameter	0.8277 ± 0.0097	0.840 ± 0.010
Planet mass (M_J)	1.92 ± 0.23	$1.910^{+0.075}_{-0.080}$
Orbital semimajor axis (AU)	0.0226 ± 0.0013	$0.02282^{+0.00023}_{-0.00040}$

I.2.3. WASP-11/HAT-P-10b

WASP-11 or HAT-P-10 (GSC 02340-01714) is an 11.89 magnitude K dwarf star located 125 parsecs away from the Solar System. Stellar parameters for WASP-11/HAT-P-10 are shown in Table V.

TABLE V. Stellar Parameters for WASP-11/HAT-P-10 from Bakos et al., 2009

Parameter	Value
RA (J2000) (h min s)	03 09 29
Dec. (J2000) (° min s)	+30 40 25
V (Magnitude)	11.89
Distance (parsec)	$125\ ^{+6}_{-5}$
$T_{\rm eff}$ (K)	4980 ± 60

WASP-11/HAT-P-10b is a sub-Jupiter sized exoplanet orbiting around WASP-11/HAT-P-10, discovered by the Wide Angle Search for Planets (WASP) Consortium (Bakos et al., 2008) and the Hungarian-made Automated Telescope (HAT) Network (West et al., 2008). The two surveys differ slightly on the precise values of planetary and orbital parameters, but the planet is approximately 1 Jupiter radius in size and half a Jupiter mass. It orbits the star in 3.72 days. A summary of the planetary and orbital parameters from both surveys is included in Table VI.

TABLE VI. Literature Values from WASP-11/HAT-P-10b Discovery Papers

Parameter	Bakos et al. (HAT)	West et al. (WASP)
Transit Epoch (BJD)	2454185.9101 ± 0.0003	2454473.05586 ± 0.0002
Orbital Period (days)	3.7224690 ± 0.0000067	$3.722465^{+0.000006}_{-0.000008}$
Planet/star radius ratio	0.1332 ± 0.0013	
Planet radius (R_J)	$1.045\ ^{+0.050}_{-0.033}$	$0.91^{+0.06}_{-0.03}$
Transit duration (days)	0.1100 ± 0.0015	$0.1065\ ^{0.001}_{-0.0003}$
Impact parameter	$0.238\ ^{+0.130}_{-0.093}$	$0.054^{+0.168}_{-0.050}$
Planet mass (M_J)	0.460 ± 0.028	0.53 ± 0.07
Orbital semimajor axis (AU)	$0.0439^{+0.0006}_{-0.0009}$	0.043 ± 0.002

I.3. Goals for Observation of Transits from Wallace Observatory

Using two of the 14-inch telescopes at the George R. Wallace Jr. Astrophysical Observatory in Westford, MA, transits of the exoplanets presented above were observed. Using the transit measurements taken, planetary and orbital parameters of each transit light curve were determined.

For each light curve, the radius of the planet was calculated, and the value from the literature were compared with this value. The midtime of the transit was also calculated. By comparing the midtime of the transit with the predicted midtime based on previous observations, the variability of the period of the orbit was determined. A variable orbital period would indicate another body in the system, such as a second planet or a large moon. The duration of the transit was also determined.

The limits of extrasolar planet observation from Wallace Observatory were evaluated. This evaluation included determining the detectability of transit timing variations, based on the precision of the transit timing in these light curves.

II. METHODS FOR EXOPLANET OBSERVATION

II.1. Preparing to Observe

A transit schedule was created with prediction software written by Elisabeth Adams (Adams, 2010). The software calculated when transits are observable from WAO by combining the timing of the transit with the altitude of the Sun, proximity and brightness of the moon, and the airmass of the target in order to determine which transits are visible each night. The highest airmass allowed was 2.0, the highest altitude of the Sun allowed was -9 degrees, and the closest distance to the moon was 30 degrees.

After determining which transits are visible, finder charts of the fields of view were created. These can be created using many different astronomical programs; for this project, the program Aladin was used to make these finder charts (Bonnarel et al. 2000). Finder charts were used for determining which transits are measurable from WAO. Specifcally, the field of view for the target should also include 'good' comparison stars, defined as stars of a comparable magnitude within the field of view. The 14-inch telescopes at WAO have a field of view of approximately 22 arcminutes, so these comparison stars must be well within that window to allow for imprecisions in telescope tracking. Also, the target star should be resolvable in the image. Most potential target stars are resolvable from the 14-inch telescopes, which have a plate scale of 1.29 arcseconds/pixel, with the exception of close binary stars such as HAT-P-1b.

Several possible observing targets were chosen because weather at the observatory prevents observations for much of the time. The process of choosing targets depends on the following criteria. First, the star must be bright enough for the telescopes to gather enough photons within about a 3-5 minute exposure time (from WAO telescopes, around V=12

is a reasonable brightness). As discussed above, other comparably bright stars should be within the field of view. Also, the transit should be deep enough to be observable with the equipment at Wallace; the minimum depth measurable from Wallace was through to be about 1% due to signal to noise calculations.

II.2. Observing at Wallace Astrophysical Observatory

The telescopes used were two nearly identical Celestron C14 Schmidt-Cassegrain telescopes (referred to in this paper as Pier 3 and Pier 4). These are mounted on equatorial Paramounts. The CCDs used were SBIG STL-1001E imaging CCD cameras with a 22x22 arcminute field of view and 1.29 arcseconds/pixel. While these telescopes are very similar, each has slightly different observing properties. For instance, the focus values on Pier 3 and Pier 4 are not identical, with Pier 3 having slightly better focus.

The R filter is generally used for transit observation, because many stars with transiting planets emit more light in redder wavelengths than in bluer wavelengths. Another benefit of the R filter is that there is significantly less background sky light at these wavelengths than in bluer wavelengths. If, however, the goal for the observation was to observe stellar limb darkening, the object was simultaneously observed on two telescopes using different filters. For instance, the V filter could be used on Pier 3 and the I filter could be used on Pier 4.

Before observations began each night, the computer clock for the telescope used was synchronized using the network time protocol (NTP). To observe any transit, data are collected throughout the transit with significant time (about 50% of the transit duration) before and after the transit event to serve as a baseline flux measurement. Collection of data takes between 2 and 8 hours, depending on the length of the transit. Dark and bias calibration frames must be taken for each observation, and flat field calibrations frames must

be taken during twilight before or after the observation.

II.3. Data Reduction

II.3.1. Calibration of CCD Frames using IRAF

The CCD frames were calibrated using the Image Reduction and Analysis Facility (IRAF)[1], a general purpose astronomical reduction and analysis software. The functions `imcombine`, `imarith`, and `imstat` were used.

Using the `imcombine` function, a dark frame was created for each exposure time using the median value of each pixel over 10-15 dark images. The dark frame for each exposure time was subtracted from each data frame of that exposure time using the `imarith` function. This calibration removes offset created by 'dark current' from the CCD, which increases with exposure time. Dark current, caused by small electric currents in the CCD even when no photons enter the device, was minimized by cooling the CCD to between -15° and -25° depending on ambient temperature conditions.

The `imcombine` function was also used to create an averaged bias frame for each filter. This bias frame was subtracted from each flat field frame (the exposure times for the flat field were all less than 1 second, so dark current is negligible). After this, the flat fields were combined for each filter using `imcombine`, taking the median value for each pixel value. Using the `imstat` function, the midpoint of the averaged flat field is calculated, and the flat field is normalized by dividing the frame by this value.

The dark-corrected frames are then divided by this normalized flat. An example of uncalibrated and calibrated CCD frames is shown in Figure 2.

[1] Image Reduction and Analysis Facility. National Optical Astronomy Observatory. http://iraf.noao.edu/

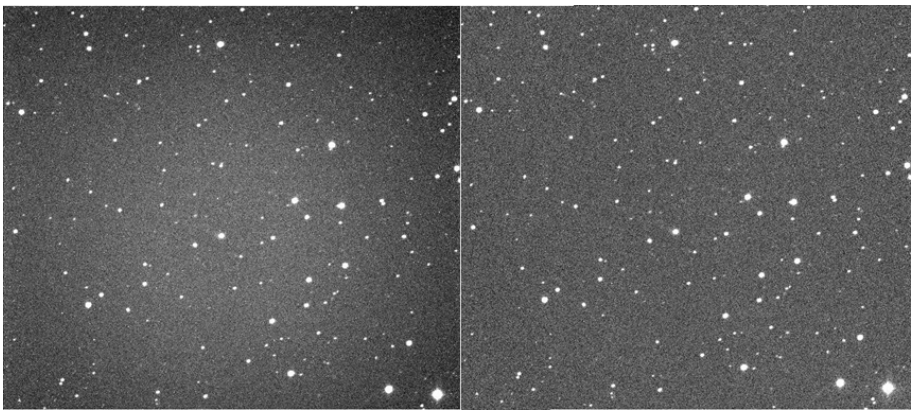

FIG. 2. **Calibrating CCD Frames.** The left image is a sample uncalibrated data frame from a WASP-10b transit that occurred on October 14th, 2009. The right image is the same frame after dark and flat calibrations have been performed. Note that the uncalibrated frame is vignetted (brighter in the middle). This effect is removed when the image is calibrated on the right.

II.3.2. Differential Photometry using IRAF and Mathematica

Differential photometry was used to determine the change in flux over time from the target star. This type of photometry compares the flux from the target star to that from other stars in the same field of view, reducing the effects of atmospheric variations.

Differential photometry was done using a combination of IRAF and a Mathematica pipeline written by Elisabeth Adams and edited for this data set.

The function `phot` from IRAF was used to do circular aperture differential photometry. The user can input a range of aperture sizes in which to enclose the object, as well as different sky sizes to subtract the background light. The `phot` function can be utilized in its interactive mode in which the user selects stars by clicking on a graphical image of the data frame, or in an automatic mode in which `phot` takes lists of files and coordinates and performs the same photometry automatically. In this case, SAOImage DS9 was used as the graphical interface. A template file was created using the interactive mode on the first data frame of the data set. The target star and all desired comparison stars were selected in this template file.

The midtime of each data file was extracted from the header file of each data frame. The template file generated by `phot` was then sent to the Mathematica pipeline. A centroiding algorithm adjusted the position of each star over time to account for imperfections in the tracking of the telescope. The pipeline returned a list of these recentered coordinates.

The IRAF function `phot` was used again, this time in its automatic mode. It read in these recentered coordinates for each data file, and returned a list of the instrumental magnitudes of the targets and comparison stars. These values included the magnitudes of the target and between 5 and 20 different comparison stars for each of the aperture sizes used, ranging from 3 pixels to 14 pixels in half steps. The sky to be subtracted from the region within this aperture was calculated using a larger annulus around each star with an inner radius input by the user.

After this, the data reduction was completed using Mathematica to produce a light curve of the magntitude ratio between the target and several chosen comparison stars. The values from the IRAF differential photometry were sent to the Mathematica pipeline. The ratio of the target to each comparison star in each aperture was calculated. The best aperture size was chosen based on calculations that minimized the scatter on points. Comparison stars that had saturated frames, too few counts, or unexplained variability in their magnitudes were eliminated. The light curve output for each data set was made by adding the contributions from each comparison star and using the ratio between the target and the sum of the comparison magnitudes. Combining stars increases photon counts, decreasing statistical uncertainty.

If the light curve had an anomaly in the baseline, some 'detrending' is possible. For instance, the anomaly could be approximately proportional to the geometric diameter of the observed star, which fluctuates due to variability in the seeing; instead, it could be

proportional to airmass because of differential extinction of the image over many hours. The light curve can be 'detrended' using a linear detrending function against geometric diameter, airmass, the x and y coordinates of the target star, or time. The function plots time versus any one of these parameters and calculates the slope. The data points are then scaled by this slope, reducing the anomaly in the baseline. This process can be repeated to detrend against other of these features present in the light curve. Many of the six light curves presented did not require detrending. Detrending of those that required it is explained in Section IV.

II.4. Transit Fitting

II.4.1. Least Squares Fit

The models were fit using a least squares fitting Mathematica package from Jim Elliot's research group at MIT. Eight different parameters were used to make this least squares fit. These parameters were the scale (the number that will normalize the baseline to 1), the slope, the midtime of the transit, the duration of the transit, the ratio of the radii of the planet and star, the impact parameter, and two limb darkening parameters. These could not all be constrained with the data from Wallace Observatory, leading to assumptions in the fit for each light curve. Different parameters were taken to be constant based on the quality of the light curve.

For all transits, the impact parameter was calculated using results from published papers. The impact parameter b is defined by the equation

$$b = \cos i \cdot \frac{a}{R_{\text{star}}}, \tag{1}$$

where i is the orbital inclination, a is the semi-major axis, and R_{star} is the stellar radius. The value of the semi-major axis a can be determined from the shape of the transit light curve. The inclination can be determined using the equation

$$t_T = \frac{PR_\star}{\pi a}\sqrt{(1+\frac{R_p}{R_\star})^2 - (\frac{a}{R_\star}\cos i)^2}, \tag{2}$$

where t_T is the transit duration and R_p is the radius of the planet (Seager 2008). The impact parameter for the fit was calculated for each transit with published values for these

parameters.

The other two values taken to be constant for all light curves were the two limb darkening parameters. These were calculated using a FORTRAN program written by John Southworth called `jktld` which accepts values for the effective temperature, surface gravity, metal abundance [M/H], and microturbulence velocity and returns values for various linear and nonlinear models for limb darkening[2]. For this fit, two quadratic limb darkening parameters are used.

The impact parameter and two limb darkening parameters were kept constant for all transit fits. In addition, values for transit duration or slope were also held constant if the transit light curve could not constrain the model well enough to fit them. The models were fit to the parameters not held constant: the scale, midtime of the transit, and the ratio of the planetary radius to the stellar radius were calculated for all light curves. (Transit duration and slope were calculated for some light curves). The initial values of the midtime and scale were estimated and input by the user; the initial values for the radius ratio and transit duration were literature values. The least squares fit algorithm iterated these initial values until they converged on a set of values that minimized the sum of the squared residuals between the model and the data. The fitting software returned the values for these parameters and the errors on the parameters from this residual of the fit.

II.4.2. Calculating Parameters using Least Squares Fit

The radius of the planet can be calculated using the ratio of the planetary radius to the stellar radius. This ratio $\frac{R_P}{R_\star}$ will be defined symbolically as δ. The planetary radius is

[2] Southworth, John. JKTLD - for calculating limb darkening coefficients. http://www.astro.keele.ac.uk/ jkt/codes/jktld.html

$$R_p = \frac{R_P}{R_\star} \cdot R_\star = \delta \cdot R_\star \tag{3}$$

with an error of

$$\Delta R_p = \sqrt{\delta^2 \cdot (\Delta R_\star)^2 + R_\star^2 \cdot (\Delta\delta)^2)}, \tag{4}$$

where $\Delta\delta$ is the error in the radius ratio from the least squares fit, $\Delta R_\star$ is the error in the radius of the star (Johnson et al. 2009), and ΔR_p is the error on the radius of the planet.

The transit midtime, transit duration, and radius ratio between the planet and the star were output with error bars. The radius of the planet was calculated using equation 4 with error bars that account for the error in the stellar radius $R_\star$. The area ratio $\frac{A_p}{A_\star}$ is defined as δ^2; the error bar is calculated by propagating $\Delta\delta$ through the equation.

III. OBSERVATIONS

Observations of the three planets discussed in the Introduction (TrES-3, WASP-10b, and WASP-11/HAT-P-10b) were taken between June 2009 and January 2010. Many other observations of other planets including HAT-P-5b, HAT-P-7b, HD17156b, HD80606b, and HAT-P-11b were attempted, but the data were discarded for a variety of reasons summarized in Table XVIII. Discussion of the difficulties experienced observing from Wallace Observatory and the viability of exoplanet research from small observatories will follow in Section VII.

TABLE VII. Reasons for Exclusion of other Transit Data

Planet	Date	Reason for Exclusion
TrES-3	2009/07/21	The night became extremely cloudy. Data were examined and images with fewer than 10,000 counts on the target star were excluded. This left approximately 20 data frames left, which were not sufficient to create a reasonable light curve.
HAT-P-5b	2009/07/07	It was hazy and the moon was extremely bright (it was a nearly full moon close to my target). The counts on the target star dropped during the night. Only a partial transit was observed.
HAT-P-7b	2009/07/10	It was clear at the beginning of the night but became cloudy. Only a partial transit was observed. In addition, the HAT-P-7b transit is shallow (0.7%) which decreased the signal to noise ratio considerably.
WASP-3b	2009/07/14	Thick clouds rolled after 30 minutes of observation. Transit was not observed.
HD17156b	2009/07/20	Observed by Robert Arlt. The night seemed to be reasonably clear; counts dropped off towards morning. The main limiting factor here is the lack of comparison stars - HD17156 is a bright star (8.17 mag) with no really comparable stars in the field. We needed 5 sec exposures to avoid saturating the target, but this meant that dimmer stars had very few counts. I used the brightest 2 stars to make this plot.
HAT-P-11b	2009/08/02	Transit was only 0.3% deep. Signal to noise ratio was extremely low, and transit was not visible within the noise.
HD80606b	2009/01/14	Observed as part of a coalition of observers organized by Josh Winn. Weather conditions at Wallace Observatory were variable and a small part of the transit was observed (part of egress plus a small amount of baseline afterwards). The light curve was sent to collaborators, but is not complete enough by itself for inclusion in this work.

III.1. TrES-3 Observations

Usable data from TrES-3 were collected on June 17th, 2009 and on July 4th, 2009. TrES-3 was a good target from Wallace Observatory for a few reasons. First, it has excellent comparison stars. Second, it is a deep transit (2.6% deep), which significantly increases the signal to noise ratio. Third, I had reasonably good weather for both transits. These observations are summarized in Table VIII. An example star field is shown in Figure 3.

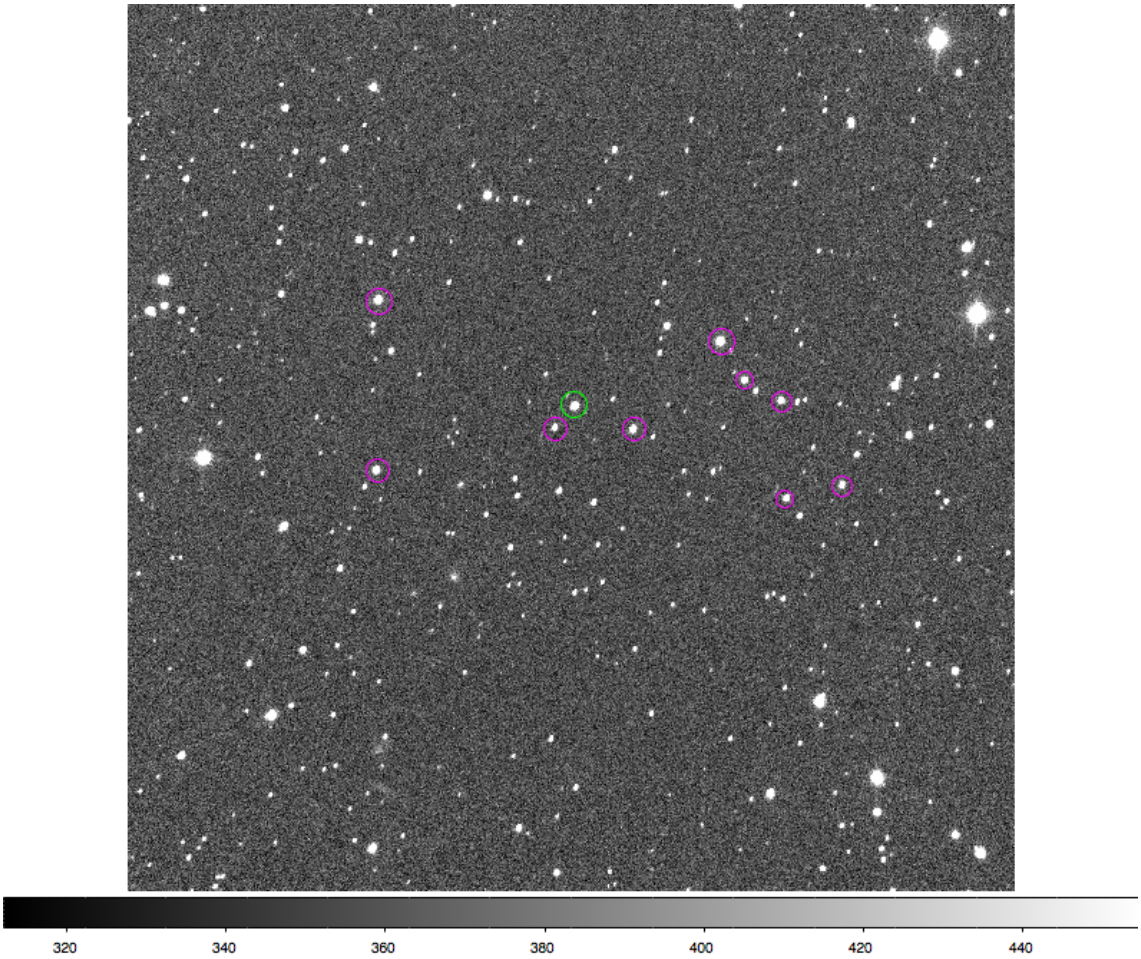

FIG. 3. **Example TrES-3 Field.** This image was taken on June 17th, 2009 and has been calibrated using flat and dark images from the same night. TrES-3 is circled in green. Comparison stars used for differential photometry are circled in magenta.

On June 17th, my very first night of observing ever, the weather was especially clear. Flats, darks, and biases were collected before observations began. The R filter was used and

TABLE VIII. Observation Log for TrES-3 Data

Date and Telescope	Frames	Type of Frame	Filter	Exposure Time (s)
2009/06/17: Pier 4	1-15	Flat	R	1-5
	16-115	TrES-3	R	75
	116-125	Dark	n/a	75
	126-135	Bias	n/a	n/a
2009/07/04: Pier 4	1-5	Flat	R	10-40
	10-11	TrES-3	R	120
	13-73	TrES-3	R	60
	77-102	TrES-3	R	75
	104-128	TrES-3	R	120
	130-135	Dark	n/a	60
	136-140	Dark	n/a	75
	141-145	Dark	n/a	120
	146-155	Bias	n/a	n/a

exposures were 75 seconds long for the whole night. The TrES-3 transit is approximately 1.3 hours long, and observations were taken for 1 hour before and after the transit.

On July 4th, the weather was slightly hazy and humid, but not cloudy. The moon was full, but in the other half of the sky from TrES-3. The observers arrived late to the observatory so the flats taken were ultimately not usable. Exposure times varied between 60 and 120 seconds as conditions varied. The R filter was used, and darks and biases were collected.

III.2. WASP-10b Observations

WASP-10 was observed for 4.5 hours, from 01:35 to 06:05 (UT) on October 14, 2009. The weather was clear and crisp. Twilight flats were obtained after the transit, during the evening of the 14th. Images were collected on two telescopes in two different filters. The I filter was used on Pier 4 and the V filter was used on Pier 3. Exposure times were varied as the seeing changed during the course of the night from 2 minutes to 3 minutes and 30 seconds. These observations are summarized in Table IX. An example star field is shown in Figure 4.

FIG. 4. **Example WASP-10 Field.** This image was taken on October 14th, 2009 and has been calibrated using dark fields from the same night and flat fields from October 15th. WASP-10 is circled in green. Comparison stars used for differential photometry are circled in magenta.

TABLE IX. Observation Log for WASP-10b Data

Date andTelescope	Frames	Type of Frame	Filter	Exposure Time (s)
2009/10/14: Pier 3	13-33	WASP-10b	*V*	150
	34-94	WASP-10b	*V*	210
	95-99	Dark	n/a	210
	100-194	Dark	n/a	150
	105-124	Bias	n/a	n/a
2009/10/14: Pier 4	1-10	Dark	n/a	60
	19-40	WASP-10b	*I*	150
	41-101	WASP-10b	*I*	210
	102-107	Dark	n/a	210
	108-112	Dark	n/a	150
	113-133	Bias	n/a	n/a

III.3. WASP-11/HAT-P-10b Observations

WASP-11/HAT-P-10b was observed for 5.5 hours from 22:30 on January 20th to 04:00 (UT) on January 21st, 2010 using both Pier 3 and Pier 4. The weather was reasonably clear, and the seeing was slightly variable. Flats were obtained during the evening before the transit. The exposure time was varied between 60 seconds and 90 seconds. The R filter was used in Pier 3 and Pier 4. Images were collected on Pier 4 for the entire 5.5 hour period. Images were collected on Pier 3 for about two thirds of the 5.5 hour transit period, with a section in the middle missing because of observer error. The observer forgot to save files automatically after the meridian flip and thus lost data between the meridian flip and the time at which she realized and fixed the mistake. These observations are summarized in Table X. An example star field is shown in Figure 5.

TABLE X. Observation Log for WASP-11/HAT-P-10b Data

Date and Telescope	Frames	Type of Frame	Filter	Exposure Time (s)
2010/01/21: Pier 3	1-61	Flat	R	0.1-5
	62-101	Bias	n/a	n/a
	102-111	Dark	n/a	60
	112-167	WASP-11/HAT-P-10	R	60
	168-306	WASP-11/HAT-P-10	R	90
	308-314	Dark	n/a	90
2010/01/21: Pier 4	1-70	Flat	R	0.1-4
	71-110	Bias	n/a	n/a
	111-120	Dark	n/a	60
	121-204	WASP-11/HAT-P-10	R	60
	205-325	WASP-11/HAT-P-10	R	90
	327-333	Dark	n/a	90

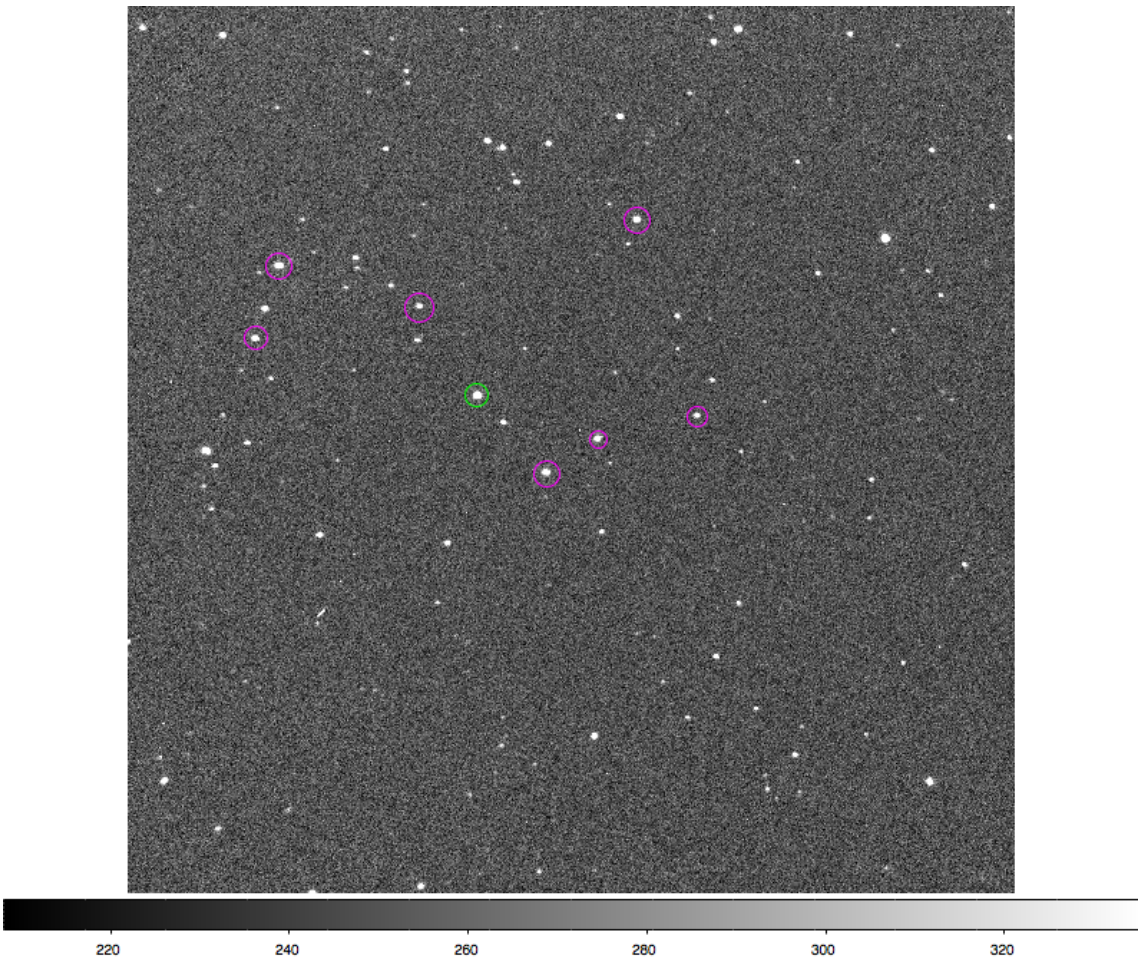

FIG. 5. **Example WASP-11/HAT-P-10b Field.** This image was taken on January 21st, 2010 and has been calibrated using flat and dark images from the same night. WASP-11/HAT-P-10 is circled in green. Comparison stars used for differential photometry are circled in magenta.

IV. DATA REDUCTION FOR OBSERVED TRANSITS

The general methods of data reduction are described in Section II.3. Each individual transit had certain deviations from the general methods that will be described in this section.

IV.1. TrES-3 Data Reduction

IV.1.1. 2009/06/17

Differential photometry for this transit used 9 comparison stars (shown above in Figure 3. The aperture size was 4.75 pixels (6 arcseconds), the sky inner radius was 17 pixels (22 arcseconds), and outer radius was 33 pixels (43 arcseconds). Frames with under 25,000 counts on the target star were removed; counts declined sharply about two thirds of the way through the transit, so the last half of the transit is noisier than the first half of the transit). The transit was detrended linearly with the geometric diameter of the target star; this detrending improved photometric precision slightly, from 2.5 mmag to 2.01 mmag.

IV.1.2. 2009/07/04

As discussed before, flats from 2009/07/04 were unusable. Instead, calibrations were done using flats from 2009/06/17. Differential photometry for this transit used 5 stars. The aperture size chosen was 4.0 pixels (5 arcseconds), the sky inner radius was 20 pixels (26 arcseconds), and the outer radius was 40 pixels (52 arcseconds). Frames with under 25,000 counts on the target star were removed. This essentially took out a cloudy middle section of the transit including ingress and the flat part after egress, leaving me with baseline before ingress and almost all of egress. The section after the meridian flip may have been

troublesome because flats from 2 weeks prior were used; this means that the fields are not completely flat because of changes in the dust and alignment of the telescope. The photometric precision of this transit was 5.44 mmag.

IV.2. WASP-10b Data Reduction

Differential photometry for WASP-10b used ten comparison stars. For both the Pier 3 and Pier 4 data, the best aperture size was 6.5 pixels (8.4 arcseconds). The sky annulus chosen had an inner radius of 25 pixels (32 arcseconds) and an outer radius of 50 pixels (65 arcseconds). The Pier 4 light curve had a slight slope that was correlated with the geometric diameter and was detrended to correct for this slope. The Pier 3 light curve did not have this slope and was not detrended against any parameters.

IV.3. WASP-11/HAT-P-10b Data Reduction

Differential photometry for WASP-11/HAT-P-10b used seven comparison stars. The aperture size chosen for both the Pier 3 and Pier 4 data was 5.5 pixels (7 arcseconds). The sky annulus had an inner radius of 30 pixels (39 arcseconds) and an outer radius of 60 pixels (77 arcseconds). The Pier 3 light curve is missing the middle section because of human error while observing (see Section III.3). The photometric precisions of the Pier 3 and Pier 4 light curves were 3.55 mmag and 3.86 mmag respectively.

V. FITTING LIGHT CURVES

V.1. TrES-3

The two TrES-3 light curves were initially fit separately from each other using the least squares fitting method described in section II.4. Limb darkening coefficients u and v were calculated to be 0.4548 and 0.1822 respectively using Claret (2000) values. For the single fits, the duration of the transit was also fixed in the fit (0.08149 days, from O'Donovan et al.) because neither light curve constrained the duration well. For the 2009/06/17 transit, the slope was fit, but for the 2009/07/04 it was held constant at zero. After these single fits were created, a multi-curve fit was created. This fit used data from both light curves to fit for planetary parameters. The duration of the transit was not held constant in the multi-transit fit because having more data constrained the duration. The results of the least squares fit for each of the single fits and the multi-transit fit are summarized in Table XI. The two fitted light curves, using the multi-transit fit, are shown in Figures 6(a) and 6(b).

TABLE XI. Results: TrES-3

Parameter	O'Donovan et al. 2007	Single Fit 20090617	Single Fit 20090704	Multi-transit fit
Pred./meas. transit time[1] (20090617)	3:58:03	04:00:37 ± 62 s		03:56:42 ± 63 s
Pred./meas. transit time[1] (20090704)	3:29:51		03:29:23 ± 114 s	03:29:43 ± 86 s
Transit duration (days)	0.08149	0.08149 (not fit)	0.08149 (not fit)	0.061 ± 0.003
Planet radius (R_J)	1.295 ± 0.081	1.46 ± 0.03	1.48 ± 0.07	1.32 ± 0.05
Orbital semimajor axis	0.0226 ± 0.0013	0.0163 ± 0.00011	0.0164 ± 0.00025	0.023 ± 0.002

[1] Predicted using midtime and period from Sozzetti et al. 2009

V.2. WASP-10b

The two WASP-10b light curves were fit separately using the least squares fitting method described in section II.4. Limb darkening coefficients were different for each light curve because the data were taken using different filters. For Pier 3 (V filter), values of u and v were 0.7657 and 0.0743. For Pier 4 (I filter), values of u and v were 0.4230 and 0.2693 using Claret (2000) values. The slopes were taken to be zero, and the light curves were fit for the four remaining parameters (radius ratio, duration, midtime, and scale). A multi-curve fit was not completed because the limb darkening coefficients were different for each light curve. The values found in each fit were then combined using a weighted average. The results of the least-squares fit for each of the single fits and the combined values using both fits are shown in Table XII. The two fitted light curves are shown in Figures 7(a) and 7(b).

TABLE XII. Results: WASP-10b

Parameter	Johnson et al. 2008	Pier 3 (V Filter)	Pier 4 (I Filter)	Combined Value
Pred./Meas. Midtime (h:min:s)[2]	4:02:44	4:03:53 ±38	4:03:34 ±35s	4:03:18 ± 26s
Transit Duration (hours)	$2.2271^{+0.0078}_{-0.0068}$	2.31 ±0.03	2.39 ±0.03	2.35 ±0.02
Planet/Star Area Ratio	$0.02525\ ^{+0.00024}_{-0.00028}$	0.0252 ±0.0008	0.0294 ±0.0008	0.0272 ±0.0006
Radius of Planet (R_J)	1.080 ± 0.020	1.08 ±0.02	1.17 ±0.03	1.12 ±0.02

V.3. WASP-11/HAT-P-10b

The two WASP-11/HAT-P10b light curves were fit separately using the least squares fitting method described in section II.4. They were then fit using the multi-transit fitting model. Limb darkening coefficients u and v were calculated to be 0.6411 and 0.1441 respectively. The slopes were taken to be zero, and the light curves were fit for the four remaining

[2] Predicted using midtime and period from Johnson et al., 2009

parameters (radius ratio, duration, midtime, and scale). A multi-curve fit was then completed, fitting both plots with the same model. The results of the least-squares fit for each of the single fits and the multi-fit values are shown in Table XIII. The two fitted light curves are shown in Figures 8(a) and 8(b).

TABLE XIII. Results: WASP-11/HAT-P-10b

Parameter	Bakos et al. 2008	Pier 4	Pier 3	Multi-fit
Predicted/measured transit time (h:m:s)[3]	01:17:21	01:16:06 ± 74s	01:15:56 ± 179s	Pier 4: 01:15:58±111s Pier 3: 01:16:56±129s
Transit duration (days)	0.1100 ± 0.0015	0.108 ± 0.002	0.111 ±0.005	0.111±0.004
Planet radius (R_J)	$1.045\ ^{+0.050}_{-0.033}$	1.106 ±0.02	1.077 ± 0.03	1.115 ±0.049
Orbital semimajor axis	$0.0439^{+0.0006}_{-0.0009}$	0.045 ± 0.001	0.0442 ±0.002	0.0415±0.002

[3] Predicted using midtime and period from Bakos et al. 2008

V.4. Plots

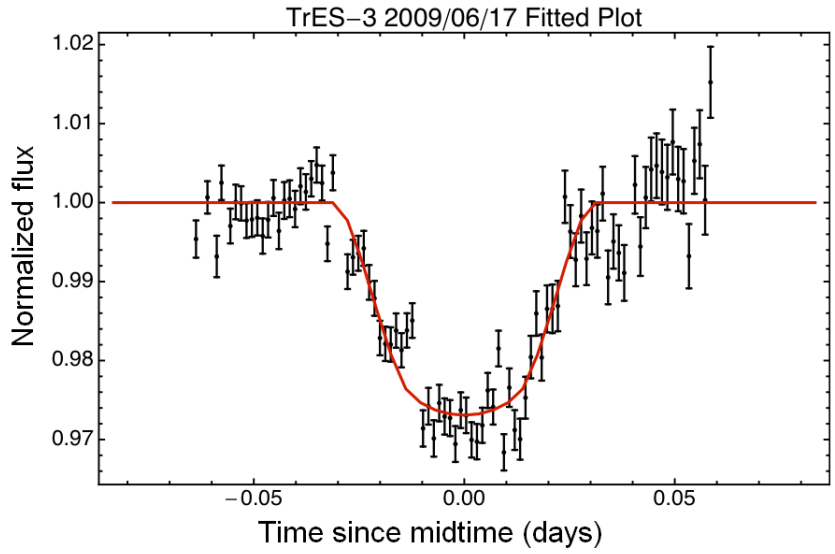

(a) **TrES-3 (2009/06/17).**

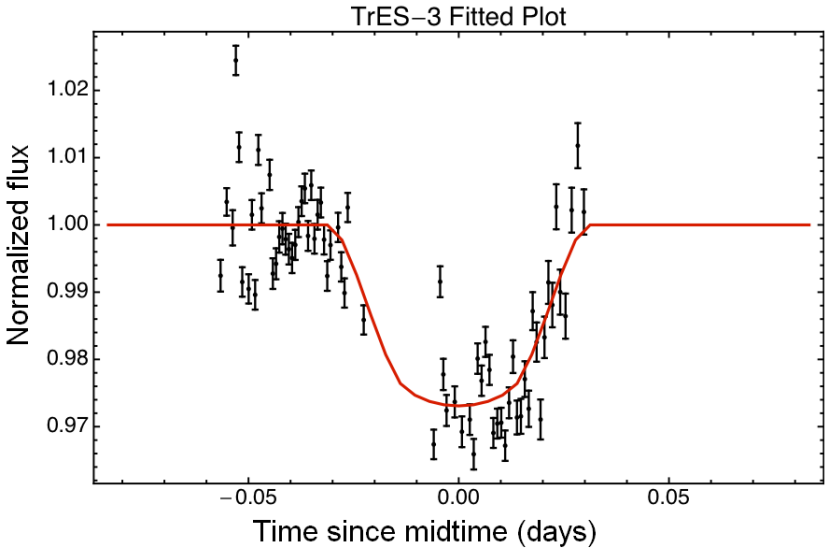

(b) **TrES-3 (2009/07/04).**

FIG. 6. The normalized flux from TrES-3 is plotted versus time from the measured midtime of the transit in days. Data points with error bars are plotted in black and the model least squares fit is plotted in red. Figure 6(a) shows data taken on June 17th, 2009 and Figure 6(b) shows data taken on July 4th, 2009 using the 14-inch Pier 4 telescope at Wallace Observatory. An R filter was used in both. The normalized flux was calculated using 9 comparison stars (top figure) and 5 comparison stars (bottom figure). The change in flux of the data during the transit is about 2.6%. Error bars show the estimated error for each data point due to photon noise. The model was fit using 4 fixed parameters and fitting for scale, midtime of the transit, duration of the transit, and the radius ratio $\frac{R_p}{R_\star}$; the same model simultaneously fit both transits. The gap in data in Figure 6(b) is due to variable clouds.

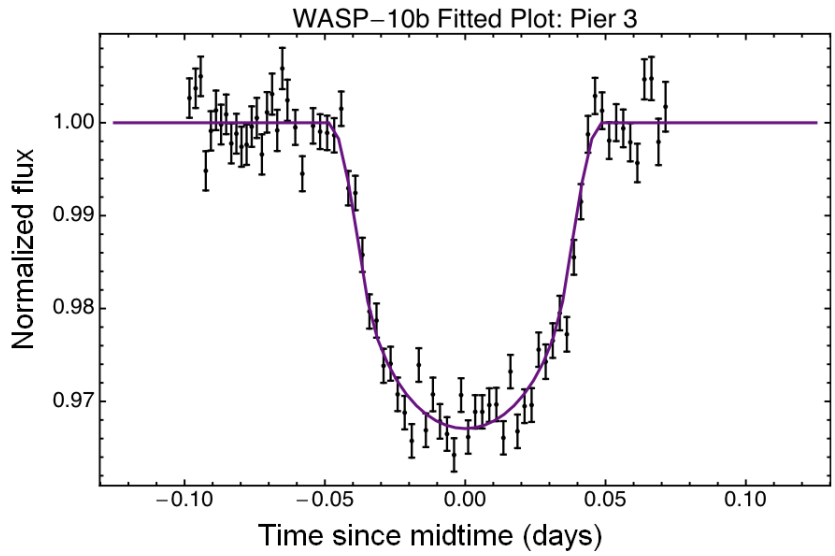

(a) **WASP-10b (*V* Filter).**

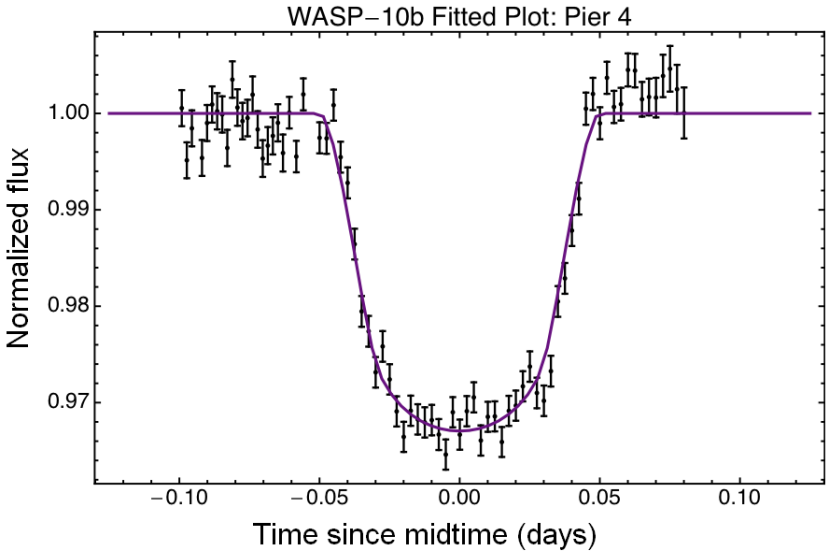

(b) **WASP-10b (*I* Filter).**

FIG. 7. The normalized flux from WASP-10 is plotted versus time from the measured midtime of the transit in days. Data points with error bars are plotted in black and the model least squares fit is plotted in purple or red. Residuals are plotted offset from the light curve. Both plots show data taken on October 14th, 2009 on 14-inch telescopes at Wallace Observatory; the data in the top plot were taken on Pier 3 and the data in the bottom plot were taken on Pier 4. A V filter was used on Pier 3 and an I filter was used on Pier 4. The normalized flux was calculated using 10 comparison stars. The change in flux of the data during the transit is about 2.5%. Error bars show the estimated error for each data point due to photon noise. The model was fit using 4 fixed parameters and fitting for scale, midtime of the transit, duration of the transit, and the radius ratio $\frac{R_p}{R_\star}$; the same model simultaneously fit both transits.

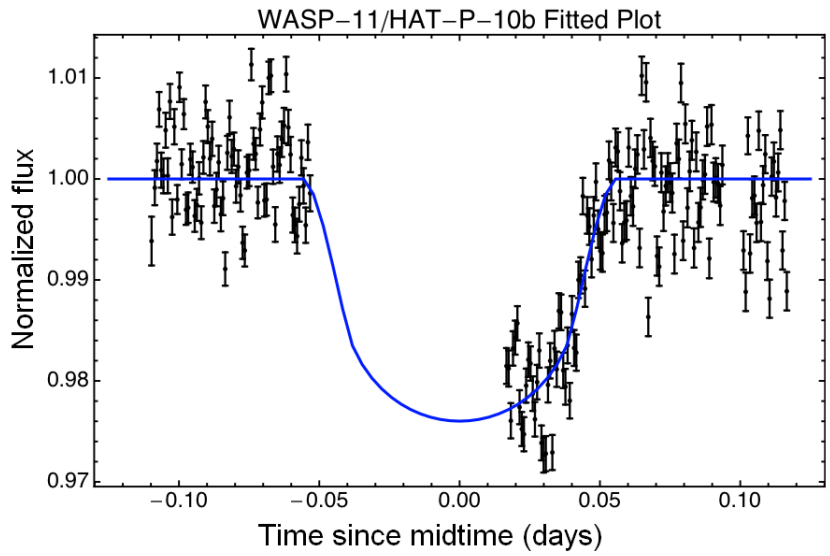

(a) **WASP-11/HAT-P-10b (Pier 3).**

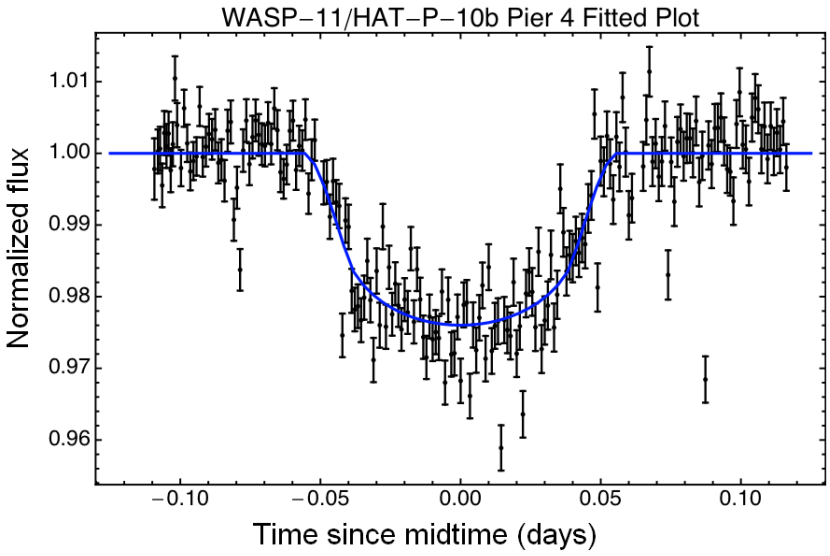

(b) **WASP-11/HAT-P-10b (Pier 4).**

FIG. 8. The normalized flux from WASP-11/HAT-P-10 is plotted versus time from the measured midtime of the transit in days. Data points with error bars are plotted in black and the model least squares fit is plotted in blue. Both plots show data taken on January 21st, 2010 on 14-inch telescopes at Wallace Observatory; the data in the top plot were taken on Pier 3 and the data in the bottom plot were taken on Pier 4. The R filter was used in Pier 3 and Pier 4. The exposure time was varied between 60 seconds and 120 seconds. The normalized flux was calculated using 7 comparison stars. The change in flux of the data during the transit is about 1.8%. Error bars show the estimated error for each data point due to photon noise. The model was fit using 4 fixed parameters and fitting for scale, midtime of the transit, duration of the transit, and the radius ratio $\frac{R_p}{R_\star}$; the same model simultaneously fit both transits.

VI. TRANSIT TIMING VARIATIONS (TTV)

VI.1. Comparing Measured Transit Midtimes with Literature Midtime Values

The deviations from predicted transit time are shown in Tables XIV, XV, and XVI and are shown graphically in the 'O-C' Figures 9, 10, and 11. These plots show the epoch of the known transit (including literature values) plotted against the observed time minus the calculated time. The code used to measure transit times and generate the plots in this section was adapted from Elisabeth Adam's transit timing code (Adams, 2010).

VI.1.1. TrES-3 TTV

As you can see, the O-C plot for TrES-3 shows that my first observed transit deviates from the calculated time by 191 seconds (2.8 sigma). Some of this difference could potentially be due to differences in calculating time in BJD. Some groups use calculations that include additional leap seconds (the code used for these calculations does) but other groups do not. (See discussion in Appendix C of Adams, 2010 for a detailed explanation of conversion between UTC and TT). The offset for all of these transits is 66.187 seconds (Adams, 2010). Whether other scientists used this offset in their calculations is difficult to determine without talking to the other groups. My second transit deviates from the calculated time by 72 seconds, which agrees within 1 sigma of the calculated time.

TABLE XIV. TrES-3 O-C Table

Transit Number	O-C (s)	Error (s)	Sigma
0	-26	26	-1.0
0	3	17	0.15
10	77	19	4.0
22	-16	24	-0.68
23	-51	18	-2.8
268	4	14	0.29
281	31	13	2.4
294	5	13	0.40
313	-53	22	-2.4
623	191	68	2.8
636	72	114	0.63

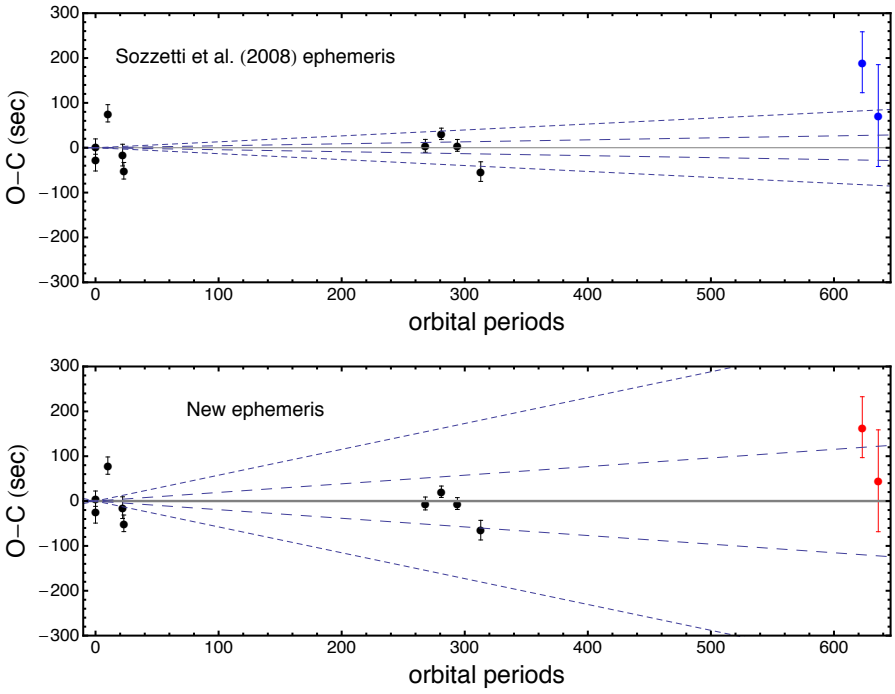

FIG. 9. **TrES-3 O minus C Graph.** This plot shows the literature midtimes of TrES-3 transits from O'Donovan et al. (2007) and Sozzetti et al. (2008). In the top plot, the period and first midtime in Sozzetti et al. (2008) was used as the baseline. The diagonal lines represent 1 sigma and 2 sigma deviations from the calculated transit time using the published error on the period. Note that Sozzetti's points and O'Donovan's points agree reasonably well with this ephemeris, though it seems that they have perhaps underestimated errors. Transits from this work are shown in blue. In the bottom plot the ephemeris is recalculated, incorporating all published midtimes plus those measured in this project. This changes the period slightly, but it greatly increases the error on the period.

VI.1.2. WASP-10b TTV

WASP-10b had the smallest statistical error bars on the timing, but the largest systematic offset from the calculated time. Note that O-C for the Pier 3 and Pier 4 were 217±35 seconds and 237±38 seconds (See Table XV and Figure 10). This could mean that a transit timing variation was detected. However, the same transit (epoch 0) was also observed by Dittmann et al. using the 61-inch Kuiper telescope on Mt. Bigelow and a clock that synchronized with GPS every few seconds (Dittmann 2010). Dittmann et al.'s value agrees very well with Christian et al. and Johnson et al.; it seems much more likely that there was some kind of systematic error in the light curve timing. One possibility is that the clock was not synchronized correctly. Another possibility is that there is a systematic error in the code that determines the timing. Preliminary fits on the data kindly provided by J Dittman (personal communication) indicate that when we fit his data using our model we do not find the same times he did, with an O-C of 469 seconds. This discrepancy is still being investigated.

TABLE XV. WASP-10b O-C Table

Transit Number	O-C (s)	Error (s)	Sigma
-246	-15	35	-0.41
-147	6	7	0.78
-111	230	69	3.3
-14	27	9	3.1
-3	244	26	9.4
-2	190	26	7.3
0	217	35	6.2
0	237	38	6.2
0	0	11	0

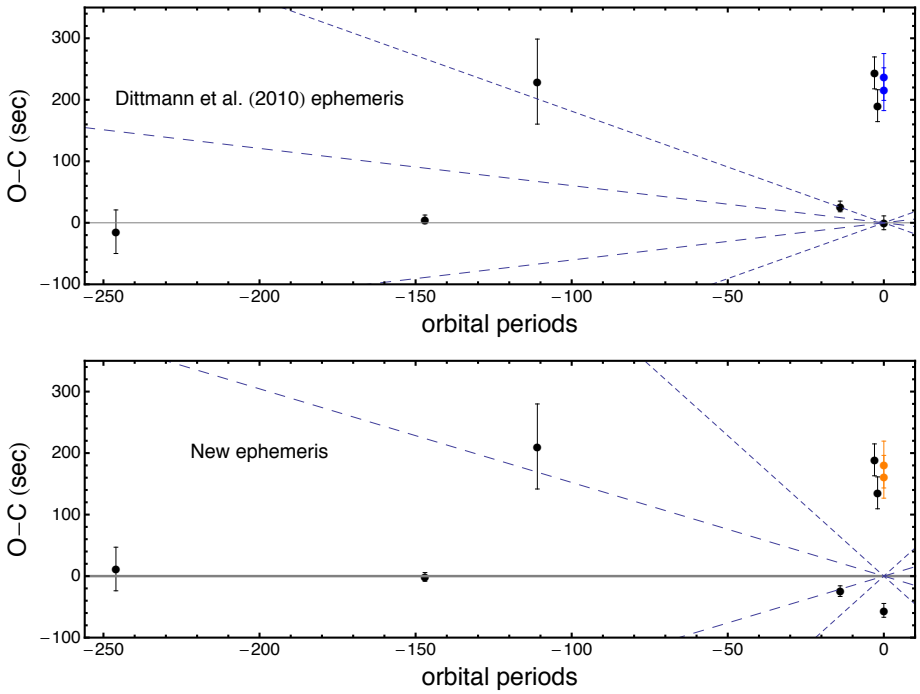

FIG. 10. **WASP-10b O minus C Graph.** This plot shows the literature midtimes of WASP-10b transits from Christian et al. (2008), Johnson et al. (2009), Krejcova et al. (2010), and Dittmann et al. (2010). In the top plot, the period and midtime in Dittmann et al. (2010) was used as the baseline. The diagonal lines represent 1 sigma and 2 sigma deviations from the calculated transit time using the published error on the period. Note that Christian's points and Johnson's points agree very well with this ephemeris; Krejcova's published points vary. The midtimes from this study are shown in blue, and deviate significantly from the ephemeris in the literature. In the bottom plot the ephemeris is recalculated, incorporating all published midtimes plus those measured in this project. This changes the period slightly, but it greatly increases the error on the period.

VI.1.3. WASP-11/HAT-P-10b TTV

The observed midtimes for WASP-11/HAT-P-10b are plotted with the two published midtimes. The first is from West et al. (2008), the WASP discovery paper. The second is from Bakos et al. (2008), the HAT discovery paper. The light curves from this paper deviate from the ephemeris from Bakos et al. by 257±179 seconds (for the partial transit, observed on Pier 3) and 268±74 seconds (for the full transit, observed on Pier 4).

TABLE XVI. WASP-10b O-C Table

Transit Number	O-C (sec)	Error (sec)	Sigma
-69	-8	17	-0.44
0	0	26	0
131	257	179	1.4
131	268	74	3.6

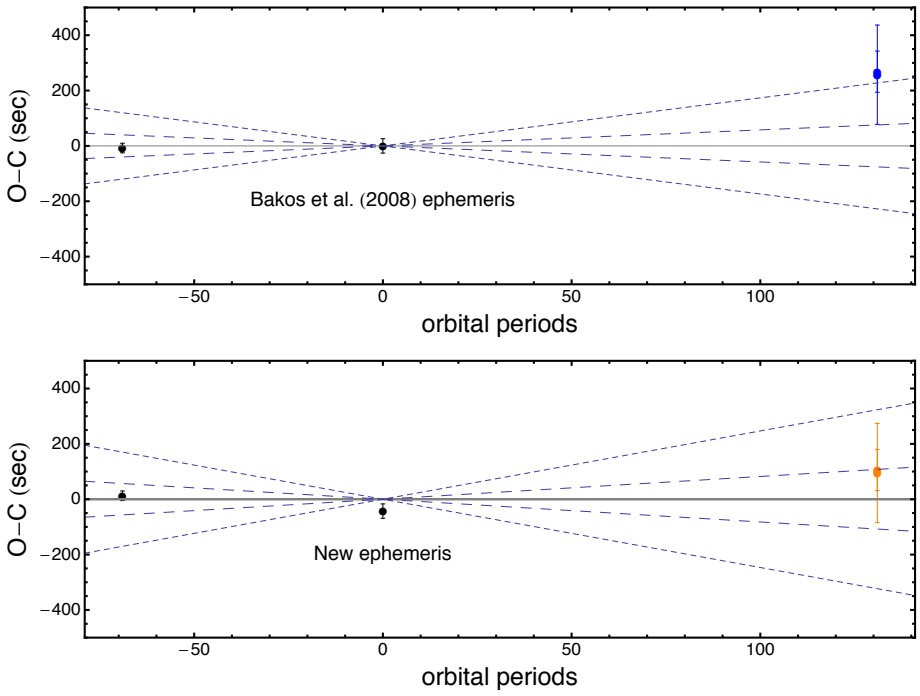

FIG. 11. **WASP-11/HAT-P-10b O minus C Graph.** This plot shows the literature midtimes of WASP-11/HAT-P-10b transits from West et al. (2008) and Bakos et al. (2008). In the top plot, the period and midtime in Bakos et al. (2008) was used as the baseline. The diagonal lines represent 1 sigma and 2 sigma deviations from the calculated transit time using the published error on the period. Note that West's points and Bakos' points agree very well with this ephemeris. The midtimes from this study are shown in blue, and deviate from the ephemeris in the literature. In the bottom plot the ephemeris is recalculated, incorporating all published midtimes plus those measured in this project. This changes the period slightly, and marginally increases the error on the period.

VI.2. Potential for Exomoon detection using Small Telescopes

In this section, the potential for exomoon discovery around TrES-3, WASP-10b, and WASP-11/HAT-P-10b will be quantified. The maximum transit timing variation that could be induced by an orbiting moon around a planet was calculated for a moon in a circular orbit around a planet which is in a circular orbit about its star. The calculations also assume there were no other perturbing influences (such as another planet) in the system. I started with Kepler's Third Law, which states

$$P^2 = \frac{4\pi^2 a^3}{G(M_s + M_p)}, \tag{5}$$

where a is the semi-major axis of the planet, M_p is the mass of the planet, M_s is the mass of the star, P is the period of the orbit, and G is the gravitational constant. The planet-moon system will rotate about its center of mass, which is located at

$$r_{cm} = \frac{d_{\text{moon}} M_{\text{moon}}}{M_p + M_{\text{moon}}}, \tag{6}$$

where r_{cm} is the distance from the planet to the center of mass, d_{moon} is the distance from the planet to the moon, and M_{moon} is the mass of the exomoon. The maximum distance the planet could be "ahead" or "behind" in its orbit would be equal to $2r_{cm}$. I then set the ratio of the perturbation in distance to the total distance equal to the ratio of the perturbation in time to the period as follows:

$$\frac{2r_{cm}}{2\pi a} = \frac{TTV}{P}, \tag{7}$$

where TTV is the maximum transit timing variation. From equations 5, 6, and 7, I determine

that the maximum TTV is

$$TTV = \frac{2d_{\rm moon}a^{1/2}}{(M_p + M_{\rm moon})G^{1/2}(M_s + M_p)^{1/2}}. \quad (8)$$

For a moon to be gravitationally bound to the planet, it must orbit within the Hill sphere of a planet. The radius of the Hill sphere is given by the equation

$$r_{Hill} = \frac{am_p}{3M_*^{1/3}}. \quad (9)$$

Moons orbiting inside the Hill sphere can be in stable orbits. Moons will not be found outside of the Hill sphere.

The precision of transit timing from Wallace for each transit was input as the TTV in this equation. The only unknowns in the equations are then $m_{\rm moon}$ and $d_{\rm moon}$. Figures 12, 13, and 14 show plots of the mass of a potential moon versus the radius at which a moon of that mass could be detected. The solid green line represents a 3σ detection. The dotted blue and magenta lines represent 2σ and 1σ detections. The shaded purple region above the green curve represents the region of detectable moons. The radius of the Hill sphere for each planet is plotted with a solid horizontal red line. The shaded red region under the red line represent the region of stable moon orbits.

For TrES-3 and WASP-10b, the region of detectable moons does not overlap with the region of stable orbits; moons under 10 Earth Masses could not be detectable using the Wallace telescopes. For WASP-11/HAT-P-10b, the region of detectable moons actually overlaps with the region of stable orbits; moons around six earth masses orbiting close to the planet's Hill Sphere could be detectable using the Wallace telescopes or other similar amateur telescopes.

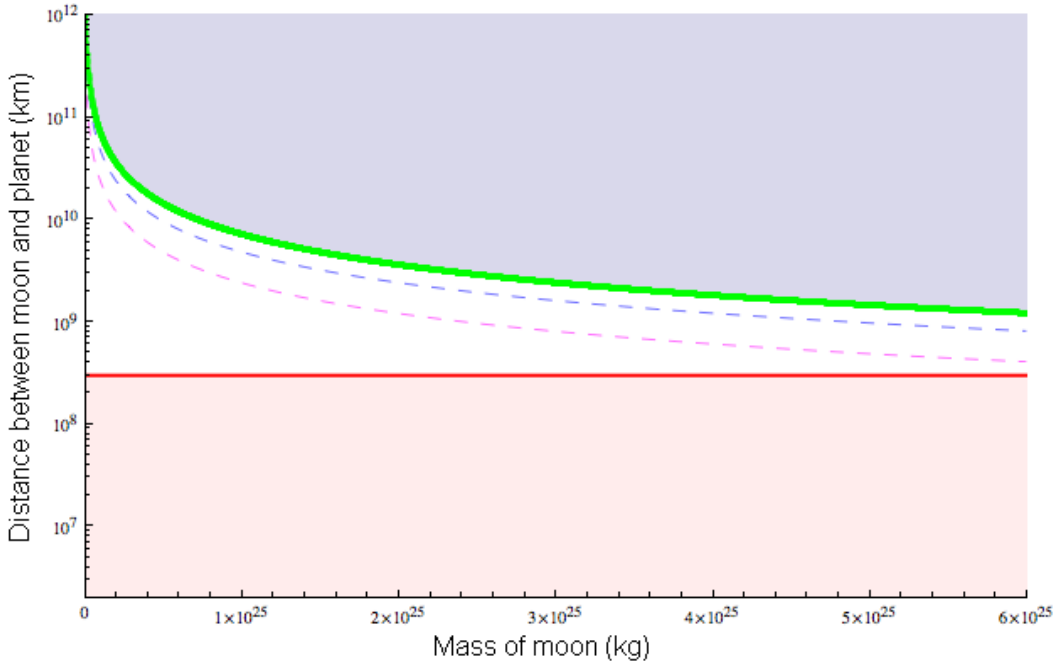

FIG. 12. **TrES-3 Detectable Moons** In this figure, the mass of a potential moon is plotted against the radius at which that sized moon could be detected. The solid green line represents a 3σ detection. The dotted blue and magenta lines represent 2σ and 1σ detections. The shaded purple region above the green curve represents the region of detectable moons. The radius of the Hill Sphere for each planet is plotted with a solid horizontal red line. The shaded red region under the red line represent the region of potentially stable moon orbits. The mass range is from 0 to 10 Earth masses. Clearly for TrES-3, the region of detectable moons does not overlap with the region of stable orbits; moons under 10 Earth Masses will not be detectable using the Wallace telescopes.

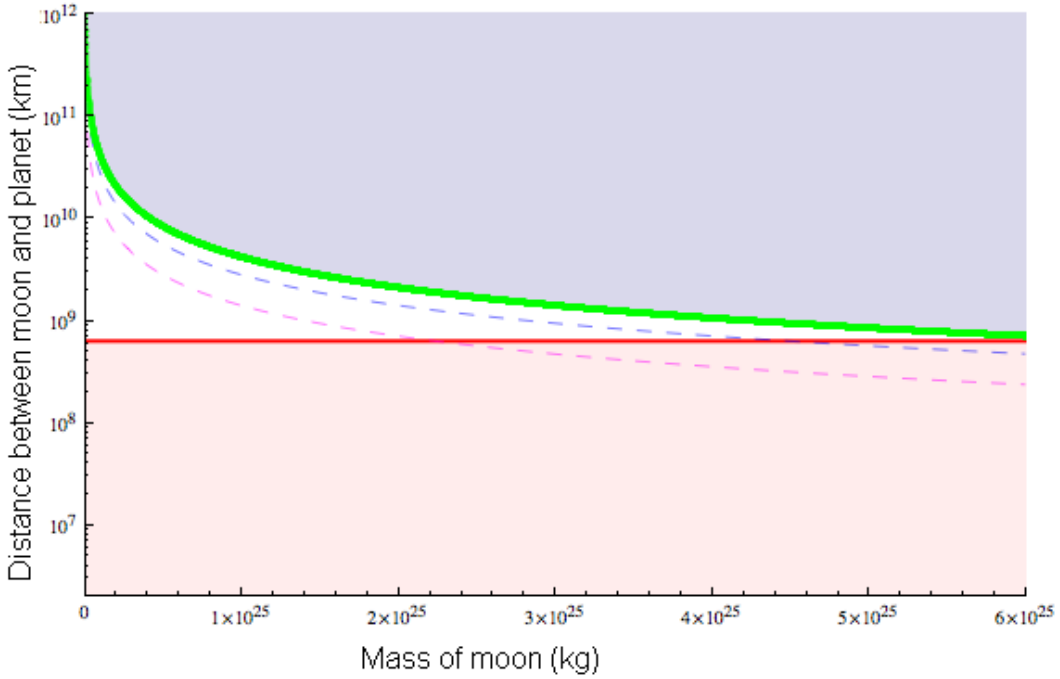

FIG. 13. **WASP-10b Detectable Moons** In this figure, the mass of a potential moon is plotted against the radius at which that sized moon could be detected. The solid green line represents a 3σ detection. The dotted blue and magenta lines represent 2σ and 1σ detections. The shaded purple region above the green curve represents the region of detectable moons. The radius of the Hill Sphere for each planet is plotted with a solid horizontal red line. The shaded red region under the red line represent the region of potentially stable moon orbits. The mass range is from 0 to 10 Earth masses. For WASP-10b, the region of detectable moons does not overlap with the region of stable orbits; moons under 10 Earth Masses will not be detectable using the Wallace telescopes.

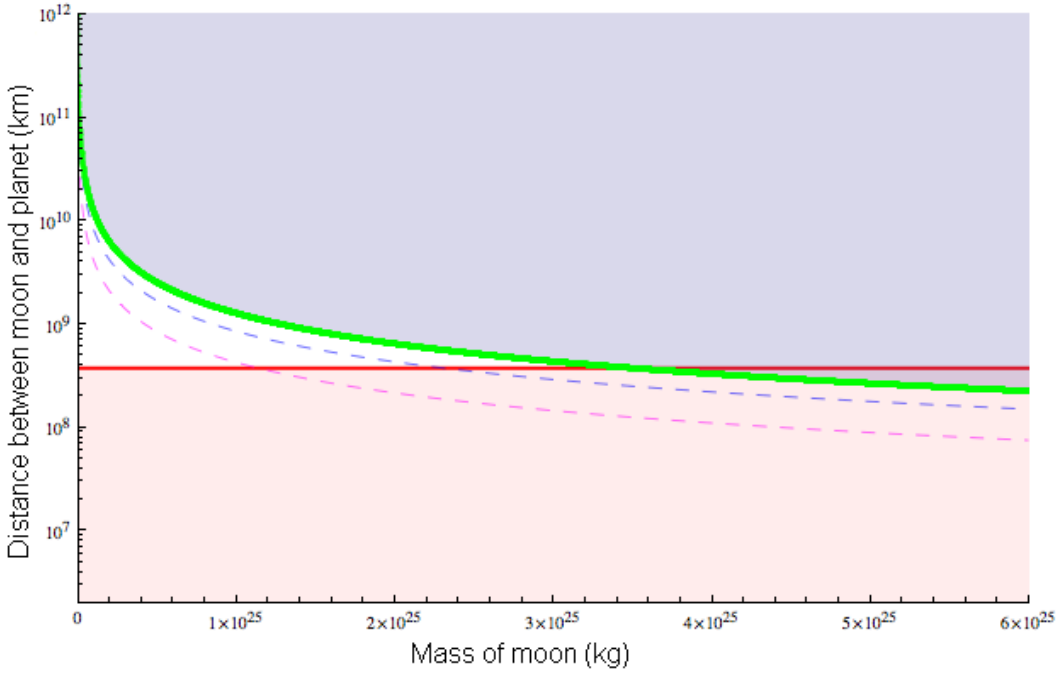

FIG. 14. **WASP-11/HAT-P-10b Detectable Moons** In this figure, the mass of a potential moon is plotted against the radius at which that sized moon could be detected. The solid green line represents a 3σ detection. The dotted blue and magenta lines represent 2σ and 1σ detections. The shaded purple region above the green curve represents the region of detectable moons. The radius of the Hill Sphere for each planet is plotted with a solid horizontal red line. The shaded red region under the red line represent the region of potentially stable moon orbits. The mass range is from 0 to 10 Earth masses. For WASP-11/HAT-P-10b, the region of detectable moons actually overlaps with the region of stable orbits; moons around six earth masses orbiting close to the planet's Hill Sphere could be detectable using the Wallace telescopes.

VII. OBSERVING CHALLENGES FROM WALLACE OBSERVATORY

As shown in Table XVIII, many observations were attempted but only a handful were successful enough to analyze to determine system parameters. In this section, the challenges of observing exoplanet transits from Wallace Observatory will be discussed. These challenges mirror those of many enthusiastic amateur astronomers attempting to observe transits using similar telescopes.

VII.1. Using Small Telescopes

The first challenge at Wallace is the size of the telescopes. I used two 14-inch telescopes for almost all of my data collection (I briefly used the 24-inch telescope, but without much luck because of poor weather conditions). These telescopes are similar in size to larger amateur telescopes. A 14-inch telescope has only 12% of the collecting area of a 1-meter telescope, or 0.3% of the collecting area of one of the 6.5 meter Magellan telescopes. This means that a 14-inch telescope collects far fewer photons than larger telescopes. While most stars with known exoplanets are plenty bright enough to be visible from these telescopes (the observation limit for both 14-inch telescopes is around magnitude 18 and stars with transits average about magnitude 12), the photon noise is much greater when fewer photons are collected.

VII.2. Location in Massachusetts

Countless observations in Westford, Massachusetts were thwarted because of the weather. Five out of seven transits discusses above in Table XVIII were omitted because of clouds or other meteorological difficulties. Many other scheduled observation sessions were not even

attempted because of clouds, rain, or snow. This is much less of a problem with larger, professional places because a location with better conditions is chosen.

Even when the weather is reasonable in Westford, the atmosphere is still a challenge. The elevation of Wallace is about 107m above sea level (in comparison, Mauna Kea, which has several telescopes, is 4,205 meters above sea level). Large telescopes are generally placed on mountaintops so that there is less atmosphere above them. The low elevation of Wallace means that the atmosphere has signficant extinction, seeing, dispersion, and scintillation effects on astronomical observations. Background light is also a problem; Wallace is near Boston, Lowell, and other urban and suburban locations.

VII.3. Examples of "Bad Data"

This section will illustrate some of the challenges encountered observing exoplanets from Wallace by showing some omitted data.

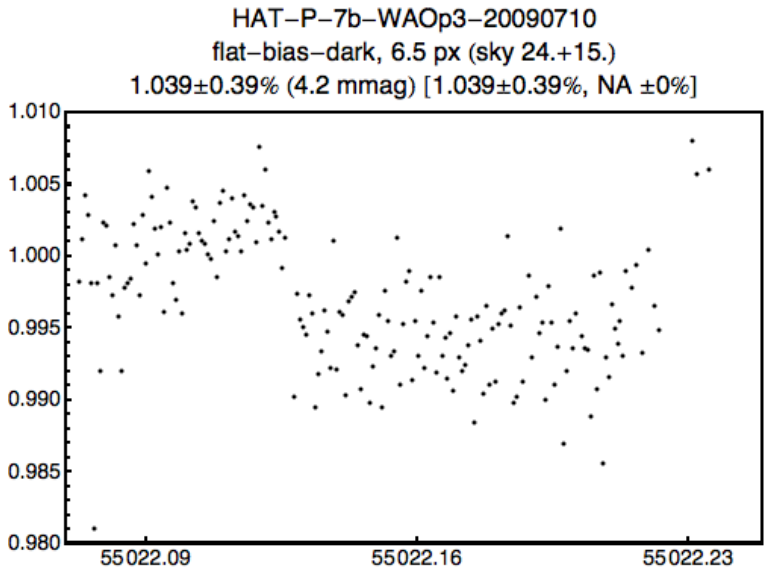

FIG. 15. **HAT-P-7b Transit.** These data were taken on July 10th from Pier 3. This transit is probably the 'best' looking rejected transit. The transit is certainly visible, and is about 0.6%. It was omitted because clouds prevented the observation of egress and because the signal to noise ratio is low because the transit is so shallow. This data illustrates that transits shallower that 0.6% are much more challenging to observe from small telescopes, especially if conditions deteriorate. Note that this transit would have been fit and analyzed if an observation of a full transit had been made.

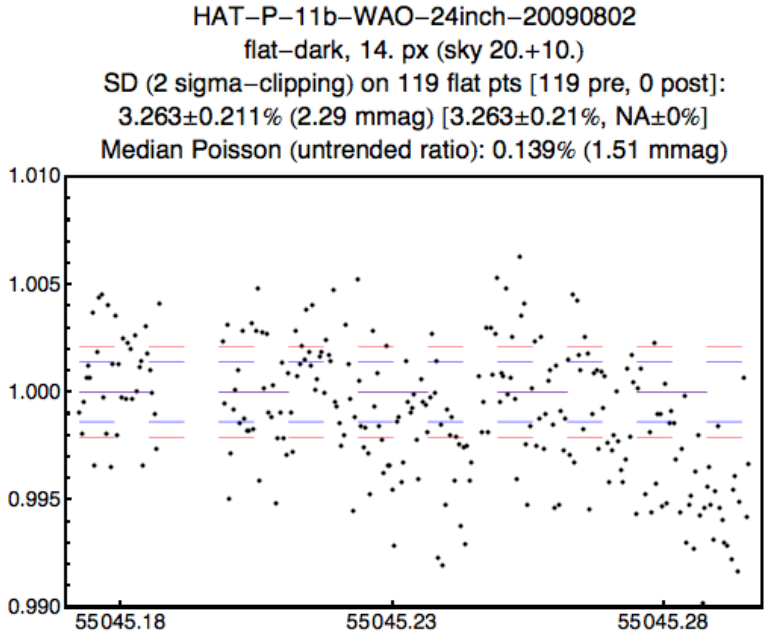

FIG. 16. **HAT-P-11b Transit.** These data were taken on August 2nd on the 24-inch telescope. There are some slightly odd systematic errors due to the non-flatness of the field, but this image is included to illustrate the limits of observation from Wallace. The transit of HAT-P-11b is 0.3% deep. Even with the 24-inch telescope, the noise here is too great to actually detect a transit this shallow.

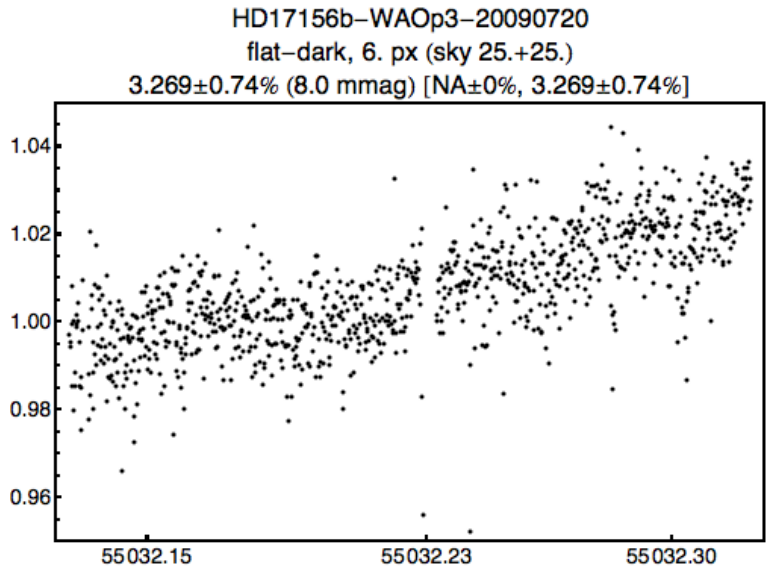

FIG. 17. **HD17156b Transit.** These data were taken on July 20th on Pier 3. There is some systematic slope. The transit of HD17156 is 0.5% deep. The limitation of this transit was not the magnitude of the target star but the magnitude of comparison stars; there were no comparably bright objects in the field. Comparison stars are challenging in this system because HD17156b is bright (V magnitude 8.17). Field of view limitations exist in all telescopes, and, in fact, the 14-inch telescopes, with 22 arcminute fields of view, are generally adequate for transits because most stars with known transiting planets are dimmer (magnitude 12).

VIII. CONCLUSIONS

I have presented six new transit light curves for three planetary systems: WASP-10b, TrES-3, and WASP-11/HAT-P-10b. The measured planetary radii and semi-major axes agree to within 1-2 sigma with literature values for all transits. The measured parameters are summarized in Table XVII.

TABLE XVII. Measured Planetary Parameters: Summary

Planet	Radius (R_J)	Semi-major Axis (AU)	Transit Duration (days)
WASP-10b	1.12 ±0.02	0.0342±0.0005	0.0979 ±0.0008
WASP-11/HAT-P-10b	1.115 ±0.049	0.0415±0.002	0.111±0.004
TrES-3	1.32 ± 0.05	0.023 ± 0.002	0.061 ± 0.003

VIII.1. Observing Exoplanet Transits and Transit Timing Variations from Small Telescopes

I have demonstrated that observing exoplanet transits from small telescopes in poor weather sites can be very successful. The transit of WASP-11/HAT-P-10b had high enough precision on its light curves to measure transit timing variations that could indicate a large ($6R_{Earth}$+) exomoon in this system.

I have also discussed the difficulties of observing transits using small telescopes. Weather conditions prevented quality observations more than 50% of the time (Out of 13 transits observations were attempted, five were ultimately discarded due to weather; dozens of others were planned but not attempted due to poor weather conditions). I determined that these 14-inch telescopes do not have enough collecting area to collect useful data for shallow transits (less than about 0.6%). This limitation would generally prevent the observation of most

small (Neptune and Earth sized) planets from Wallace and other small observatories. Some small planets could be detectable around small stars like M dwarfs because the same planet creates a deeper transit when it crosses in front of a star with a smaller radius. GJ 1214b (Charbonneau et al., 2009) is an example of such an object; while the planet is approximately Neptune-sized, its transit it 1.4% deep. Because of its smaller mass, a 3σ detection of a 1 Earth mass moon around GJ 1214b could be made, assuming a TTV precision of about 75 seconds (about the timing precision of the WASP-11/HAT-P-10b transits presented here). The measurement of this transit was planned for March/April 2010 but not executed due to a combination of poor weather and time constraints.

Another limitation discovered during this process is the limitation in transit timing accuracy. While the WASP-10b transits measured had a respectable precision (30-40 seconds), they differed by several minutes from the measurement made by Dittmann et al. on the same night. This difference indicates that in order to trust midtimes of transits to be correct, the timing of the frames should be better synchronized — probably GPS triggered, like the POETS camera which was designed to measure occultations, eclipses, and transits (Souza et al., 2006). This would certainly be possible to install on small telescopes and would make the timing measurements much more standardized and reliable.

VIII.2. Future Observations

Increasing the accuracy of transit timing on amateur telescopes and at teaching observatories such as Wallace Observatory would create a wealth of useful transit timing data. The precision of the best light curves from Wallace, about 30-40 seconds, is small enough to detect large moons. Furthermore, there are millions of small telescopes much like those at Wallace spread across the world. If the data collected on these telescopes could be standard-

ized to a global time by GPS and collected in an automatic pipeline, the data could easily be used to detect moons or other planets in the system without using telescopes larger than 1 meter.

IX. APPENDIX

TABLE XVIII. All Attempted Transit Observations

System	UT Date	Telescope	Filter	Hours	Observer	Used?
TrES-3	2009/06/17	Pier 4	R	3	CVM	yes
TrES-3	2009/07/04	Pier 4	R	3	CVM	yes
HAT-P-5b	2009/07/07	Pier 3	R	5	CVM	no
HAT-P-7b	2009/07/10	Pier 3	R	5	CVM	no
WASP-3b	2009/07/14	Pier 4	R	2	CVM	no
HD17156b	2009/07/20	Pier 3	R	7	RAA	no
TrES-3	2009/07/21	Pier 3/4	R	3	CVM	no
HAT-P-11b	2009/08/02	24-inch	R	6	CVM	no
WASP-10b	2009/10/14	Pier 3/4	R	4.5	CVM	yes
HD80606b	2009/01/14	Pier 3/4	R	8	CVM	no
WASP-11/HAT-P-10b	2009/01/21	Pier 3/4	R	5.5	CVM	yes

X. WORKS CITED

Adams, E. Transit Timing with Fast Cameras on Large Telescopes. PhD Thesis, MIT, 2010.

Bakos, G et al., HAT-P-10b: A light and moderately hot Jupiter transiting a K dwarf. 24 Sep 2008. arXiv:0809.4295v2 [astro-ph].

Christian et al., WASP-10b: a 3MJ, gas-giant planet transiting a late-type K star. Mon. Not. R. Astron. Soc. 392, 15851590 (2009).

Dittman, J. et al., Transit Observations of the WASP-10 System. 9 March 2010. arXiv:1003.1762v1 [astro-ph.EP].

Holman, M. J. & Murray, N. W. 2005, Science, 307, 1288

Johnson, J et al., 2009 A Smaller Radius for the Transiting Exoplanet WASP-10b. *ApJ* 692 L100.

Krejcova, T. et al., Photometric observation of transiting extrasolar planet WASP-10b. 5 March 2010. arXiv:1003.1301v1 [astro-ph.EP].

O'Donovan, F. et al., TrES-3: A Nearby, Massive, Transiting Hot Jupiter in a 31 Hour Orbit. 2007 ApJ 663 L37.

Southworth, John. JKTLD - for calculating limb darkening coefficients. http://www.astro.keele.ac.uk/ jkt/codes/jktld.html

Souza, Steven P. POETS: Portable Occultation, Eclipse, and Transit System. Publications of the Astronomical Society of the Pacific, 118: 15501557, 2006 November.

Sozzetti, A. et al., A New Spectroscopic and Photometric Analysis of the Transiting Planet Systems TrES-3 and TrES-4. 26 Sep 2008. arXiv:0809.4589v1 [astro-ph].

The Extrasolar Planets Encyclopaedia. Web. 02 May 2010. http://exoplanet.eu/

West, R. et al., The sub-Jupiter mass transiting exoplanet WASP-11b. *Astronomy & Astrophysics* Sep 17 2008.